

Usher syndrome and Leber congenital amaurosis are molecularly linked via a novel isoform of the centrosomal ninein-like protein

Erwin van Wijk^{1,2,7}, Ferry F.J. Kersten^{1,2,3,4,7}, Aileen Kartono^{2,4}, Dorus A. Mans², Kim Brandwijk², Stef J.F. Letteboer², Theo A. Peters^{1,7}, Tina Märker⁵, Xiumin Yan⁶, Cor W.R.J. Cremers^{1,7}, Frans P.M. Cremers^{2,4}, Uwe Wolfrum⁵, Ronald Roepman^{2,4,*} & Hannie Kremer^{1,4,7*, Ψ}

Departments of ¹Otorhinolaryngology, ²Human Genetics and ³Ophthalmology, Radboud University Nijmegen Medical Centre, Nijmegen, The Netherlands. ⁴Nijmegen Centre for Molecular Life Sciences, Radboud University Nijmegen, Nijmegen, The Netherlands. ⁵Department of Cell and Matrix Biology, Institute of Zoology, Johannes Gutenberg University of Mainz, Mainz, Germany. ⁶Department of Cell Biology, Max-Planck Institute of Biochemistry, Martinsried, Germany. ⁷Donders Centre for Neuroscience, Nijmegen, The Netherlands.

* Both authors contributed equally to this work.

Ψ Corresponding author: Hannie Kremer, Department of Otorhinolaryngology, Radboud University Nijmegen Medical Centre, internal postal code 377, P.O. Box 9101, 6500 HB Nijmegen, The Netherlands. Tel.: +31.24.3610487; Fax.: +31.24.3668752.

Email: h.kremer@antrg.umcn.nl

ABSTRACT

Usher syndrome (USH) and Leber congenital amaurosis (LCA) are autosomal recessive disorders resulting in syndromic and nonsyndromic forms of blindness. In order to gain insight into the pathogenic mechanisms underlying retinal degeneration, we searched for interacting proteins of USH2A isoform B (USH2A^{isoB}) and the *LCA5*-encoded protein lebercilin. We identified a novel isoform of the centrosomal ninein-like protein, hereby named Nlp isoform B (Nlp^{isoB}), as a common interactor. Although we identified the capacity of this protein to bind calcium with one of its three EF hand domains, the interaction with USH2A^{isoB} did not depend on this. Upon expression in ARPE-19 cells, recombinant Nlp^{isoB}, lebercilin, and USH2A^{isoB} were all found to colocalize at the centrosomes. Staining of retinal sections with specific antibodies against all three proteins revealed their co-localization at the basal bodies of the photoreceptor connecting cilia. Based on this subcellular localization and the nature of their previously identified binding partners, we hypothesize that the pathogenic mechanisms for LCA and USH show significant overlap and involve defects in ciliogenesis, cilia maintenance, and intraflagellar and/or microtubule-based transport. The direct association of Nlp^{isoB} with USH2A^{isoB} and lebercilin indicates that *Nlp* can be considered as a novel candidate gene for USH, LCA and allied retinal ciliopathies.

INTRODUCTION

Usher syndrome (USH) is the most common cause of combined deaf-blindness with a prevalence of about 1 in 20,000 in the Caucasian population (1-3). It is a clinically and genetically heterogeneous disorder, for which three different types can be distinguished based on the severity and progression of the hearing loss, the presence or absence of vestibular symptoms and the age of onset of retinitis pigmentosa (RP) (4). To date, six different genetic loci have been identified for USH type I (USH1), three loci for USH type II (USH2) and one locus for USH type III (USH3) (reviewed in (5)). Mutations have been identified in the genes encoding myosin VIIa, harmonin, cadherin 23, protocadherin 15, and SANS as the underlying defect in USH1b, -c, -d, -f and -g, respectively (6-11). Defects in USH2A, GPR98 (VLGR1) and whirlin are causative for USH2a, -c and -d, respectively (12-15). USH3 is caused by mutations in the clarin-1 encoding *USH3A* gene (16).

Recently, we and others have shown that all known USH1 and USH2 proteins are present in a protein network, the Usher interactome, in which harmonin and whirlin play the role of key organisers that interconnect the other USH proteins (17-22). Localization studies in rodents revealed that this interactome is present in the stereocilia and the synaptic region of hair cells in the cochlea, and in the synaptic region of photoreceptor cells. Except for harmonin, all known USH1 and USH2 proteins are also present at the region of the connecting cilium of photoreceptor cells, a microtubule-based structure which separates the outer segments from the inner segments (21). This region encompasses the connecting cilium, its basal body and centriole as well as the periciliary region surrounding the connecting cilium. In the region of the connecting cilium, the Usher interactome may be recruited via PDZ (postsynaptic density 95, PSD-95; discs large, Dlg; zonula occludens-1, ZO-1) domain based interactions with whirlin (19,21,23). Based on the localization of the Usher protein network to the region of the connecting cilium and the identification of ciliary abnormalities in photoreceptor cells and sperm cells of several patients with USH (24), the syndrome can be considered as a (retinal) ciliopathy (25). Recent phenotypic data of patients with different Usher subtypes (USH 1B, 1F, 2A or 2C) also suggests that the primary pathogenic insult does not take place at the photoreceptor synapse (26).

Leber congenital amaurosis (LCA) is another clinically and genetically heterogeneous recessive disorder which has been described as a severe form of retinitis pigmentosa presenting before the age of one year with the absence of photoreceptor function (27). Patients present with profound visual loss, nystagmus, poorly reactive pupils and a markedly

diminished or non-detectable electro-retinogram (27,28). Defects in the centrosomal and cilia-associated proteins RPGRIP1, CEP290 and lebercilin (encoded by *LCA5*) have been identified to be associated with LCA (29-31), implicating a role of these proteins in ciliary processes.

At the moment, mutations in several different genes have been described to be the underlying cause of USH and LCA, but the molecular basis of the pathogenic defects of these syndromes still remains largely elusive. Based on similarities in clinical manifestations and the subcellular localization of proteins involved in USH and a number of proteins involved in LCA, the pathogenic mechanisms underlying both disorders might significantly overlap. In order to gain a better insight into the molecular basis of USH and LCA we searched for novel interacting partners of the recently identified lebercilin (*LCA5*) and the intracellular region of USH2A^{isoB} by using yeast two-hybrid screening.

In this study we show that both lebercilin and the intracellular region of USH2A^{isoB}, directly interact with a novel isoform of the second member of the ninein-family, the centrosomal ninein-like protein (Nlp^{isoB}), encoded by the *Nlp* (*KIAA0980*) gene. Nlp^{isoB} is a novel component of the Usher interactome, connecting USH and LCA at the molecular level, and the *Nlp* gene can therefore be considered as a novel candidate for USH, LCA, and related disorders.

RESULTS

A novel isoform, isoform B, of the centrosome associated Ninein-like protein interacts with USH2A and lebercilin

Yeast two-hybrid screens of an oligo d(T) primed human retina cDNA library were performed to identify proteins interacting with lebercilin or with the intracellular region of USH2A^{isoB}. Analysis of positive clones that activated all reporter genes, revealed a common interactor for both bait proteins. In total, eleven overlapping clones of a novel splice-variant of the centrosomal ninein-like protein (Nlp), hereby named Nlp isoform B (Nlp^{isoB}), were identified. By using the intracellular region of USH2A^{isoB} as a bait, two clones for Nlp^{isoB} were identified. These encode amino acids 598-1033 and 658-1033, respectively. For lebercilin, four Nlp clones encoding amino acids 598-1033 and five clones encoding amino acids 658-1033 were identified. The transcript encoding Nlp^{isoB} lacks exon 17 from the originally described *Nlp* gene, resulting in in-frame skipping of 349 amino acids after residue 734. The specificity of the interaction in the yeast two-hybrid assay was determined by co-transforming pAD-Nlp^{isoB} (aa 658-1033) with the pBD-Gal4 vector expressing the non-related p63 protein. No interaction was observed performing this control experiment (data not shown).

Bioinformatic analysis of the Nlp^{isoB} protein (SMART database; <http://smart.embl-heidelberg.de/>) identified three regions that are predicted to form EF hand domains, potentially Ca²⁺-binding, which are known to be involved in the interaction with γ -tubulin (32). In addition, the C-terminal region was predicted to form an intermediate filament (IF) domain (aa 656-925), likely to be involved in protein-protein interactions (Pfam Home Page; <http://pfam.sanger.ac.uk/>) (Fig 1A). The intermediate filament domain, however, was predicted with low significance (E-value: 5.2×10^{-1}). We analyzed the spatial and temporal expression pattern of transcripts encoding Nlp^{isoA} and Nlp^{isoB} by semi-quantative RT-PCR, using several human fetal and adult tissues. No major differences in expression were observed for isoforms A and B, indicating that both isoforms function in the same tissues (Fig. 1B). However, differences at the cellular level cannot be excluded.

Deletion constructs were made of the intracellular region of USH2A^{isoB} and Nlp^{isoB} and tested in yeast two-hybrid analysis to determine the regions that are involved in the interaction. By using these deletion constructs we were able to show that in USH2A, the interacting region is located in the fragment containing amino acids 5124-5196 and in Nlp^{isoB} in the fragment containing the predicted intermediate filament domain (aa 656-925) (Fig. 2A).

In order to further pinpoint the domains involved in the interaction between Nlp^{isoB} and lebercilin, parts of the lebercilin protein comprising the amino acids 1-95, 96-305, 306-490 and 491-697 were tested in a yeast two-hybrid assay with different parts of Nlp^{isoB}. This revealed that the predicted intermediate filament domain of Nlp^{isoB} specifically interacts with the fragment encompassing the first two coiled-coil domains of lebercilin (aa 96-305) (Fig. 2B). To test whether the interactions of USH2A^{isoB} and lebercilin with Nlp are isoform-specific, a liquid β -galactosidase assay was performed using both Nlp^{isoA} and Nlp^{isoB} together with lebercilin and the intracellular region of USH2A^{isoB}. A specific interaction was observed between both proteins and Nlp^{isoB}, whereas no interaction with Nlp^{isoA} could be detected (Fig. 2C and D).

Co-immunoprecipitations were performed to confirm the interaction between USH2A and Nlp^{isoB}. For this purpose, COS-1 cells were co-transfected with constructs encoding HA-tagged Nlp^{isoB} and the flag-tagged intracellular region of USH2A (USH2A_{tail}). From the COS-1 cell lysates we were able to co-immunoprecipitate HA-tagged Nlp^{isoB} and flag-tagged USH2A with antibodies against the flag-tag. As a negative control, unrelated flag-tagged STRAD was co-expressed with HA-tagged Nlp^{isoB}. As expected, HA-tagged Nlp^{isoB} and flag-tagged STRAD did not co-immunoprecipitate (Fig. 3A). The interaction between lebercilin and Nlp^{isoB} could be confirmed in a GST pull-down experiment and in co-immunoprecipitation assays. We were able to pull down flag-tagged lebercilin from a COS-1 cell lysate with GST-fused Nlp^{isoB} but not with GST alone (Fig. 3B). In addition, we were able to co-immunoprecipitate flag-tagged Nlp^{isoB} and HA-tagged lebercilin with antibodies against the HA-tag. As a negative control, unrelated flag-tagged LRRK2 was co-expressed with HA-tagged lebercilin. No LRRK2 was co-immunoprecipitated with lebercilin (Fig. 3C). Also, co-immunoprecipitation assays of endogenous proteins were performed from bovine retinal extracts by using antibodies against lebercilin and Nlp. We were able to co-immunoprecipitate Nlp with an antibody against lebercilin. As a negative control, rabbit IgGs were used (Fig. 3D).

The interaction between USH2A and Nlp is calcium-independent

Because of the predicted presence of three EF-hand domains in the N-terminal half of Nlp, we hypothesized that the interaction between USH2A^{isoB} and Nlp^{isoB} might be dependent on the binding of Ca²⁺ ions to these EF-hands, as was shown for the interaction between the EF-hand domain containing proteins centrin and transducin (33). Therefore, we first determined the Ca²⁺-binding capacity of Nlp. At residue twelve of EF-hand domains, an

invariant Glu or Asp provides two oxygens for liganding Ca^{2+} (bidentate ligand) (34). Based on this, only EF-hand 3 would be able to efficiently bind Ca^{2+} (Fig. 4A). To test this hypothesis, GST fusion proteins were made of the three predicted EF hands of Nlp. As a positive control, the GST-fused calmodulin 28K subunit was used. We indeed were able to show binding of Ca^{2+} to Nlp EF hand 3 and not to EF hands 1 and 2 (Fig. 4B). Subsequently, we performed GST pull-down assays in the presence or absence of 2 mM CaCl_2 in which HA-tagged full length Nlp isoform B was pulled down from a COS-1 cell lysate with GST-USH2A_tail but not with GST alone. Also, no HA-tagged Nlp^{isoB} was pulled-down with GST-fused NBC3_tail. NBC3 was used as an additional negative control, and is a previously described member of the Usher interactome (17). Similar results were obtained for pull-down experiments performed in the presence or absence of calcium and therefore there are no indications for calcium-dependence of the interaction (Fig. 4C).

Nlp co-localizes with USH2A^{isoB} and lebercilin at the photoreceptor cell basal body and centriole

We performed immunohistochemistry for Nlp and USH2A^{isoB} to determine whether both proteins co-localize in the retina. Monoclonal anti-*pan-centrin* antibodies (20H5) were used as a marker for the basal body and connecting cilium. With affinity purified antibodies against Nlp, the presence of Nlp was detected in the inner segment and at the basal body, shown as a partial co-localization with centrins (Fig. 5B). On retinal cryosections Nlp and USH2A^{isoB} co-localized in the inner segments and at the region of the connecting cilium (Fig. 5A). In addition, USH2A^{isoB} localized to the outer plexiform layer as was already described (17,19).

To determine the exact subcellular localization of Nlp in the retina, immunoelectron microscopy was performed. We detected Nlp in the basal body and the centriole of the photoreceptor connecting cilium as well as in periciliary region of the apical inner segments of mouse photoreceptor cells (Fig. 5C). Immunoelectron microscopy for USH2A^{isoB} on the retina showed the presence of USH2A^{isoB} in the periciliary region, the connecting cilium, basal body and the centriole of photoreceptor cells (Fig. 5D; (21)). Immunohistochemistry on mouse retinal cryosections revealed lebercilin as a component of the photoreceptor connecting cilium and basal body (29). Thus, our results indicate that Nlp co-localizes with USH2A^{isoB} and also with lebercilin at the photoreceptor cell basal body.

Nlp, lebercilin and USH2A co-localize at the centrosome of ARPE-19 cells

Cashenghi and coworkers have shown that Nlp localizes at the mother centriole of the centrosome in cells during interphase (32). In order to visualize the interaction between the intracellular domain of USH2A and Nlp^{isoB}, we fused these proteins at their N-terminus to enhanced cyan fluorescent protein (eCFP) and monomeric red fluorescent protein (mRFP), respectively. In single transfected human retinal pigment epithelium cells (ARPE-19) expressing Nlp^{isoB}, this protein shows a centrosomal localization specifically at one centriole, most probably the mother centriole (Fig. 6A). In mitotic cells a punctate localization in the cell periphery was observed for Nlp^{isoB} (data not shown). In single transfected cells a nuclear localization (data not shown; (17,19)), or a centrosomal localization was observed for eCFP-USH2A (Fig. 6B). In cells co-expressing Nlp^{isoB} and USH2A, co-localization was observed at both the mother and the daughter centriole of the cell (Fig. 6D-D''). In addition, overexpression assays in ARPE-19 cells were performed by co-expressing N-terminally fused mRFP-Nlp^{isoB} and C-terminally fused lebercilin-eYFP. In single transfected cells, lebercilin-eYFP was localized to the centrosome and microtubule network of the cell, as previously described (29) (Fig. 6C). In cells co-expressing Nlp^{isoB} and lebercilin-eYFP, co-localization at the centrosome and non-centrosomal microtubule organization centres (MTOC's) was observed (Fig. 6E-E'').

To determine the subcellular localization of endogenous Nlp and lebercilin, ARPE-19 cells were induced to form primary cilia by serum starvation and subsequently used for immunohistochemical stainings with antibodies directed against Nlp and lebercilin. Both proteins could be detected at the base of the cilium, most probably the basal body (Fig. 7A,B). Interestingly, we detected both lebercilin and Nlp at the midbody during cytokinesis (Fig. 7C,D). After telophase, the mother centrioles which are present at the midbody develop into the basal bodies of the newly formed cells (35). No endogenous USH2A was detected in ARPE-19 cells.

Lebercilin mutations affect the interaction with Nlp^{isoB}

Recently, we have identified truncating lebercilin mutations in LCA patients (29). We addressed the biologic relevance of the interaction between lebercilin and Nlp^{isoB} by testing the effect of two of these mutations, p.Q279X and p.P493TfsX1, on the association with Nlp^{isoB}. In a quantitative yeast two-hybrid interaction assay the p.Q279X mutation significantly enhanced the interaction. The interaction of Nlp^{isoB} and the p.P493TfsX1 mutant was found to be completely abolished (Fig. 8A).

The subcellular localization of the lebercilin mutants was studied upon expression in ciliated ARPE-19 cells. When expressed alone, mRFP-tagged lebercilin localizes to the basal body, the primary cilium and the microtubule network of the cell (Fig. 8B;(29)). The mRFP-lebercilin^{Q279X} mutant does not associate with the microtubule network any longer but is present in the primary cilium and its basal body (Fig. 8C). In contrary, mRFP-lebercilin^{P493TfsX1} only localizes to the microtubule network in the cell periphery but no longer to the cilium and basal body (Fig. 8D). Co-expression of Nlp^{isoB} and lebercilin showed a clear co-localization, specifically at the basal body (Fig. 8E-E’’). In the primary cilium and the microtubule network, only lebercilin was present. As indicated by the yeast two-hybrid assay, the interaction between Nlp^{isoB} and lebercilin^{Q279X} is enhanced. When co-expressed with Nlp^{isoB}, lebercilin^{Q279X} is recruited to the basal body, but is no longer observed in the primary cilium (Fig. 8F-F’’). Upon co-expression of Nlp^{isoB} and lebercilin^{P493TfsX1} no co-localization was observed, confirming the loss of interaction between the two proteins (Fig. 8G-G’’). These data indicate that truncating mutations in lebercilin severely affect the association with Nlp at the basal body. However, downregulation of both endogenous *Nlp* and *LCA5* by RNAi in ciliated ARPE-19 cells does not result in altered protein localization of Nlp or lebercilin (Supplementary Fig. S2), suggesting that additional binding partners are involved in their localization at the basal body.

Discussion

In this study, we demonstrate that a novel isoform of the centrosome-associated ninein-like protein, Nlp^{isoB}, specifically interacts with lebercilin and the cytoplasmic region of USH2A, thereby linking Usher syndrome and Leber congenital amaurosis at the molecular level. Previous analysis of *Xenopus laevis* Nlp already suggested the presence of two Nlp isoforms, which correspond with human Nlp^{isoA} and Nlp^{isoB} (36). Nlp is the second member of the ninein protein family and has a 37 % sequence identity with ninein (32). Nlp is predominantly present in the mother centriole of the centrosome and in the basal body of primary cilia in cultured cells, and is involved in microtubule-nucleation, -anchoring and -outgrowth (32,36,37). However, it remains to be elucidated which isoform of Nlp is present and functions at these subcellular structures. The interaction between USH2A^{isoB}, lebercilin and Nlp^{isoB} and their co-localization in the basal bodies, the centrioles and the periciliary compartments of photoreceptor cells shows that at least Nlp^{isoB} molecules are present there.

Basal bodies and associated centrioles are found at the base of cilia and serve as a nucleation site for the axonemal and cytoplasmic microtubules, respectively (38,39). The photoreceptor cell outer segment is regarded as a highly specialized cilium corresponding to the ciliary shaft of a prototypic cilium (38,39). The connecting cilium then correlates with the short junction between the basal body and axoneme of a prototypic cilium, the transition zone (38). The presence of Nlp at the basal bodies and centrioles of the ciliary apparatus of photoreceptor cells matches with the previously determined localization of Nlp in the basal body of ciliated cells (36). Based on the knowledge on Nlp function in mitotic cells (32,36,37), we propose that Nlp functions in the development and maintenance of the connecting cilium and outer segment and in the establishment of a microtubule network in (the apical part of) the inner segment in differentiated photoreceptor cells.

In addition to the physical interaction of both USH2A^{isoB} and lebercilin with Nlp^{isoB}, similarities in clinical manifestations between USH and LCA suggest a significant overlap in the pathogenic mechanisms underlying both disorders. Based on the subcellular localization and the current knowledge on USH2A^{isoB} and lebercilin, these pathogenic mechanisms are likely to include ciliary dysfunction. Post-mortem observation of connecting cilium defects in the retina and the identification of sperm abnormalities in some USH patients (reviewed in (40)), as well as the involvement of other cilia-associated proteins in non-syndromic forms of retinal degeneration and USH, contribute to this hypothesis (19,24,29,30,41,42). Two proteins involved in (non-)syndromic retinitis pigmentosa, RPGR and RP1, and even the LCA-associated proteins RPGRIP1 and CEP290, have been shown to localize to the connecting cilia of photoreceptor cells, emphasizing the role of impaired cilia function in the pathogenesis of retinal degeneration (30,43-46).

The connecting cilium of photoreceptor cells connects the inner and outer segments. Within the outer segments the actual phototransduction takes place. Since protein synthesis does not occur in the outer segments, the proteins essential for phototransduction and assembly and maintenance of the axonemal and outer segment structure are transported through the connecting cilium between the inner segment and the outer segment, analogous to the intraflagellar transport (IFT) (47,48). In cilia and flagella, IFT complexes are assembled near the basal body and transported along the axoneme by the heterotrimeric kinesin II (KIF3A/3B/KAP3) and the homodimeric KIF17 in an anterograde direction and back to the basal body region by cytoplasmic dynein 2/1b (49-52). In photoreceptor cells, IFT20, IFT52, IFT57 and IFT88 molecules and both kinesin motors are thought to be present in an anterograde transport complex (53-55). Dysfunction of the components of the IFT transport

complex lead to mislocalization of structural proteins and proteins involved in the phototransduction and subsequently lead to retinal degeneration (53,56). This is corroborated by the development of both polycystic kidney disease in addition to retinal degeneration in mice after the introduction of a hypermorphic mutation in IFT88 (53,57). Also, photoreceptor-specific silencing of KIF3A leads to mislocalization of opsin and arrestin, proteins involved in phototransduction (56). Similar defects were observed in mice lacking *BBS4*, a gene involved in Bardet-Biedl syndrome (58). *BBS4* is a member of the recently discovered BBSome, which is required for ciliogenesis and is hypothesized to function in IFT and vesicular transport to the cilium (59). The evaluation of the cellular function of USH proteins in photoreceptors suggests the participation of these proteins in the transport through the connecting cilium (21,48,60,61). Also, there is growing evidence that BBS molecules, IFT proteins and USH proteins participate in microtubule-based vesicular transport through the cytoplasm (21,53,59,62). The molecular links of Nlp^{isoB} with the USH2A^{isoB} and lebercilin proteins qualified these as common denominators in the associated retinal protein network, suggesting that common molecular processes are disrupted in the retinas of USH2A and LCA5 patients. We indeed were able to determine that protein truncating mutations in lebercilin affect the interaction with Nlp, but as downregulation of expression of any of these proteins by RNAi had no effect on the localization of the interacting partner, the physiological defect is more complex and remains to be identified. The USH2A-associated protein network, the lebercilin interactome (29) and the Nlp interactors p150^{glued} and Plk1 (32,36,37) provide multiple links with centrosomal and ciliary processes and pathways that are now potentially connected through Nlp.

Recently, we and others showed the presence of the Usher protein network in a periciliary collar-like structure at the apical part of the photoreceptor inner segments, analogous to the periciliary ridge complex of *Xenopus* photoreceptor cells, and the Usher proteins were hypothesized to function in transport and docking of vesicles containing proteins for the outer segment (21,23,63). These cargo vesicles originate from the trans-Golgi network of the photoreceptor cells and are thought to be transported along microtubules by cytoplasmic dynein through the inner segment to the apical membrane (21,64). Nlp might function in this vesicular transport by the direct association with the dynactin p150^{glued} subunit of the dynein-dynactin motor complex (37), explaining the presence of Nlp in the inner segments of photoreceptor cells. The periciliary region and also the basal body and centriole are thought to serve as a docking site from where ciliary proteins (e.g. IFT proteins and proteins involved in signalling) are further distributed (65). In such a model, Nlp would

function as the molecular switch between intracellular and IFT transport. The effect of mutations in lebercilin on its interaction with Nlp^{isoB} and on its localization in the cilium are in line with this model.

Interestingly, Nlp is known to be phosphorylated by Polo-like kinase 1 (Plk1) (32,36,37), which is a key regulator in centrosome function. Plk1 also phosphorylates nucleophosmin (66), a centrosome-associated protein that acts in nucleocytoplasmic shuttling (67) and is a member of the previously identified lebercilin-interactome (29). In addition, nucleophosmin associates with RPGR-ORF15, a protein involved in X-linked retinal degeneration (68). The Nlp-interacting protein p150^{glued} (37) was found in a protein complex with RPGR-ORF15 and with lebercilin (29,69). The direct or indirect association of Nlp with several protein complexes in the region of the photoreceptor connecting cilium, stresses the importance of this protein in photoreceptor cell function.

In conclusion, our data show that USH and LCA are molecularly linked by the direct association of USH2A^{isoB} and lebercilin with a novel isoform of Nlp, Nlp^{isoB}. Co-localization of these proteins at the basal body of photoreceptor cells and the current knowledge on the function of the existing Usher protein network(s) point towards an interdependent function for Nlp^{isoB}, USH2A^{isoB} and lebercilin, possibly in cytoplasmic trafficking and ciliary transport of proteins involved in photoreception. We propose that at the basal body, Nlp^{isoB} could function as a molecular hinge connecting cytoplasmic transport mechanisms to the IFT transport machinery, suggesting an important role for Nlp in photoreceptor cell function. The central position of Nlp in the protein network indicates that *Nlp* can be considered as an excellent candidate gene for Usher syndrome, LCA or other (retinal) ciliopathies. However, no pathogenic mutations have been identified so far.

MATERIAL AND METHODS

Animals and tissues

In this study mature Wistar rats and C57BL/6J mice housed in standard cages and receiving water and food *ad libitum*, were used. Animal experiments were conducted in accordance with international and institutional guidelines. Bovine retinas were dissected from eye balls obtained from the local slaughterhouse (21).

Plasmids and antibodies

Affinity purified polyclonal antibodies directed against Nlp were described before (32). Monoclonal antibodies recognizing centrins 1-4 (20H5), polyclonal antibodies directed against the cytoplasmic region of USH2A, and affinity purified polyclonal antibodies directed against lebercilin were previously described (17,19,29). The immunohistochemical stainings of Nlp and USH2A were specific. No staining was observed after pre-adsorption of the primary antibodies with the corresponding peptide epitope. In addition, primary Nlp antibodies did not recognize GFP-tagged ninein after Western blot analysis (Supplementary data S1). Anti-flag, anti-HA, anti-acetylated tubulin and anti-gamma tubulin antibodies were purchased from Sigma (Germany). Anti-HA beads were purchased from Roche (Germany). Secondary antibodies for immunohistochemistry and western blot analysis were purchased from Molecular Probes-Invitrogen (USA), Rockland (USA), and Jackson ImmunoResearch Laboratories (USA). cDNA encoding (parts of) the cytoplasmic region of human USH2A (Genbank NP_996816) (aa 5064-5202, 5064-5168, 5064-5196, 5124-5196, 5124-5202 and 5169-5202) were cloned in the pDONR201 vector using the Gateway cloning system (Invitrogen, USA) according to manufacturers instructions. cDNA fragments of the human *Nlp* gene were amplified by using IMAGE clone IRATp970C1131D (RZPD, Germany) as a template. By using Gateway technology (Invitrogen, USA), cDNAs encoding human full length Nlp^{isoB} (aa 1-1033) (Genbank EU718622), Nlp^{isoA} (aa 1-1382) (Genbank NM_025176), the predicted EF hand domains (aa 11-39, 200-228 and 237-265), the predicted intermediate filament domain (aa 656-925) of Nlp^{isoB} and deletion constructs for Nlp^{isoB} encoding aa 599-1033, aa 656-1033 and aa 656-825, were cloned in the pDONR201 vector. Lebercilin fragments (Genbank NP_859065) encoding aa 1-95, 96-305, 306-490 and 491-697 were amplified by PCR, using pDONR201-lebercilin^{fl} as a template, and cloned in pDONR201 (29).

Yeast two-hybrid analysis

A GAL4-based yeast two-hybrid system (HybriZAP, Stratagene, USA) was used to identify proteins that interact with the cytoplasmic region of USH2A^{isoB} (aa 5064-5202) and proteins that interact with lebercilin (aa 1-697), using methods previously described (70) with minor variations. Yeast strain PJ69-4 α (71) was used as a host, which carried the *HIS3* (histidine), *ADE2* (adenine), *MEL1* (α -galactosidase) and *LacZ* (β -galactosidase) reporter genes. The DNA-binding domain fused to the human USH2A cytoplasmic region (pBD-USH2A_{tail}) and fused to full length lebercilin (pBD-lebercilin^{fl}) were used as a bait for screening a human oligo-d(T) primed retina cDNA library containing 1.9×10^6 primary clones fused to the activation domain (pAD). In total, 1.1×10^7 clones (USH2A) and 5.0×10^7 clones (lebercilin) were plated on amino acid dropout plates lacking Trp, Leu and His (SD -WLH plates), containing 1 mM 3-aminotriazol (3-AT), and selected for growth. Clones were then patched on medium additionally lacking adenine (SD -WLHA plates), and selected for growth and α -galactosidase activity by the activation of the *MEL1* reporter gene. The latter was done using 20 μ g/ml of the chromogenic substrate 5-Bromo-4-Chloro-3-indolyl α -D-galactopyranoside (X- α -Gal) in the dropout plates, and selecting the yeast cells that developed a blue-green colour due to hydrolysis of X- α -Gal by the secreted α -galactosidase enzyme. Further selection of positive clones was based on β -galactosidase activity by the activation of the *LacZ* reporter gene, that was detected by a filter lift assay, as previously described (70).

Liquid β -galactosidase assay

Three independent clones of PJ69-4 α yeast cells co-transformed with pAD-Nlp^{isoA} full length or Nlp^{isoB} full length and pBD-USH2A_{tail} or pBD-lebercilin full length were cultured in selective medium lacking Trp and Leu (SD-WL). After two overnight incubation steps at 30°C, the optical density of the cultures was determined at a wavelength of 600 nm. Cell lysis and subsequent colorimetric reactions were performed by using the Yeast β -galactosidase assay kit (Pierce, USA) according to manufacturer's instructions. Absorbance was measured at a wavelength of 420 nm.

Expression analysis

The expression of Nlp^{isoA} and Nlp^{isoB} was examined by performing semi-quantitative RT-PCR analysis on RNA from human fetal and adult tissues as described before (72). Primers used for the detection of the transcripts encoding Nlp^{isoA} are 5'- GAGGGGGAGACCAAATAGC -3' and 5'- TCTGAATGGTCACACGATGC -3'. For detection of Nlp^{isoB} the following primers were used: 5'- ACCTGCAGCAGATCAGACTG -3' and 5'- TGATTTGGTCACTCTGCTG -3'. Samples were taken after 25, 30 and 35 cycles.

Calcium binding assay

GST-fusion proteins of the predicted Nlp EF hands 1 (aa 11-39), 2 (aa 200-228) and 3 (aa 237-265) were produced by transforming BL21-DE3 cells with pDEST15-Nlp EF hand 1, 2 and 3. Precleared lysates were separated on precasted 4-12% NuPage gradient gels (Invitrogen, USA) and subsequently blotted onto nitrocellulose membranes. The membranes were incubated for 10 minutes at room temperature with 10-20 $\mu\text{Ci/l}$ ⁴⁵CaCl₂ (New England Nuclear, USA) in 10 mM imidazole, pH 6.8, and 60 mM KCl. The blots were washed twice for 5 minutes with 50% ethanol, dried and subsequently exposed to a radiation sensitive film (Kodak, Germany) (73).

GST pull-down assay

In order to produce GST (glutathion S-transferase) fusion proteins, BL21-DE3 cells were transformed with pDEST15-USH2A_tail (aa 5064-5202), pDEST15-NBC3_tail (aa 1119-1214) and pDEST15-Nlp^{isoB} (aa 1-1033). Cells were induced at 30°C for 4 hours with 0.5 mM IPTG and subsequently lysed with STE buffer (1% Sarkosyl, 1% Triton-X-100) supplemented with protease inhibitor cocktail (Roche, Germany). Lysates were precleared and incubated at 4°C for 16 hours with glutathione Sepharose 4B beads (Amersham Biosciences, USA). Beads with bound fusion proteins were washed twice with lysis buffer and three times with TBSTD (TBS with 1% Triton-X-100 and 2 mM DTT). During each washing step, samples were incubated on a rotating wheel at 4°C for 5 minutes. The amount of bound GST-fusion protein was verified on a 10% SDS-PAGE gel stained with Gelcode Blue Stain Reagent (Pierce, USA). HA-tagged Nlp^{isoB}, 3xflag-tagged lebercilin, 3xflag-tagged USH2A_tail and 3xflag-tagged NBC3_tail were produced by transfecting COS-1 cells with, respectively, pcDNA3-HA-Nlp^{isoB}, p3xflag-lebercilin, p3xflag-USH2A_tail and p3xflag-NBC3_tail using Nucleofector kit V (Amaxa, USA), program A-24 according to manufacturer's instructions.

The precleared supernatants were incubated overnight at 4°C in the presence or absence of 2 mM CaCl₂ with equal amounts of blocked beads with GST, or beads with GST-fusion proteins. After three washes with lysis buffer, the beads were boiled in 1xSDS loading buffer. Protein complexes were resolved on 4-12% NuPage gradient gels (Invitrogen, USA). For Western blot analysis, proteins were electrophoretically transferred onto nitrocellulose membranes, blocked with 5% non-fat dry milk (Biorad, Germany) in PBST (0.1% Tween) and analyzed with the appropriate primary and secondary antibodies in 0.5% milk in PBST. Bands were visualized using the Odyssey Infrared Imaging System (LI-COR, USA). Tagged molecules were detected by anti-HA or anti-flag mono- or polyclonal antibodies. As secondary antibodies IRDye800 goat-anti-mouse IgG (Rockland, USA) and Alexa Fluor 680 goat-anti-rabbit IgG were used (Molecular Probes, USA).

Co-immunoprecipitation from COS-1 cells

HA-tagged Nlp^{isoB} and HA-tagged lebercilin were expressed by using the mammalian expression vector pcDNA3-HA/DEST. Flag-tagged intracellular region of USH2A, flag-tagged Nlp^{isoB} and flag-tagged LRRK2 were expressed by using p3xflag-CMV/DEST from the Gateway cloning system (Invitrogen, USA). Both plasmids contain a CMV promoter. COS-1 cells were (co-)transfected by using Effectene (Qiagen, Germany) according to manufacturer's instructions. Thirty hours after transfection, cells were washed with PBS and subsequently lysed on ice in lysis buffer (50 mM TRIS-HCl pH 7.5, 150 mM NaCl, 0.5% Triton X-100) supplemented with complete protease inhibitor cocktail (Roche, Germany). HA-tagged Nlp^{isoB} and lebercilin were immunoprecipitated from cleared lysates overnight at 4°C by using rat monoclonal anti-HA beads (Roche, Germany) whereas flag-tagged USH2A_{tail}, Nlp^{isoB} and LRRK2 were immunoprecipitated by using polyclonal anti-flag antibodies (Sigma, Germany) and Protein A/G PLUS-sepharose (Santa Cruz Biotechnology, USA). After 4 washes in lysis buffer, the protein complexes were resolved on 4-12% NuPage gradient gels (Invitrogen, USA) and subsequently analyzed on immunoblots as described for the GST pull-down assay. Bands were visualized by using the Odyssey Infrared Imaging System (LI-COR, USA). Tagged molecules were detected by anti-HA or anti-flag mono- or polyclonal antibodies. As secondary antibodies IRDye800 goat-anti-mouse IgG (Rockland, USA) and Alexa Fluor 680 goat-anti-rabbit IgG were used (Molecular Probes, USA).

Co-immunoprecipitations from bovine retinal extracts

For immunoprecipitations, bovine retinas from a local slaughterhouse were used. Retinas were lysed by sonification (2 times 30 seconds) in lysisbuffer (50 mM Tris-HCl pH 7.4, 150 mM NaCl, 0.5% Nonidet-P40, 1 mM Natrium-orthovanadate) supplemented with complete protease inhibitor cocktail (Roche, Germany). Lysates were precleared and incubated for 16 hours at 4°C with mouse monoclonal anti-rabbit IgGs, rabbit polyclonal Nlp antibodies or polyclonal rabbit lebercilin antibodies. Protein-antibody complexes were coupled to Protein A/G PLUS-sepharose beads (Santa Cruz, USA) for 2 hours at 4°C. After incubations, the beads were pelleted and washed three times with lysis buffer. Beads were boiled and proteins were resolved on 4-12% NuPage gradient gels (Invitrogen, USA) and subsequently analyzed on immunoblots as described for GST pull-down. Bands were visualized using the Odyssey Infrared Imaging System (LI-COR, USA).

Co-localization analyses in ARPE-19 cells

To determine the cellular localization of the cytoplasmic region of human USH2A, full length lebercilin and full length Nlp^{isoB} in ARPE-19 cells, cDNAs encoding the region of USH2A in pDEST501 were cloned by using the Gateway cloning technology (Invitrogen, USA), resulting in N-terminally fused eCFP-USH2A. Nlp was cloned in pDEST733, resulting in N-terminally fused mRFP-Nlp^{isoB}. Lebercilin was cloned in pDEST504, resulting in C-terminally fused lebercilin-eYFP. ARPE-19 cells were cotransfected with pDEST733- Nlp^{isoB} and pDEST501-USH2A_tail or pDEST504-lebercilin by using Effectene (Qiagen, Germany) according to manufacturer's instructions. Twenty hours after transfection, cells were washed with PBS, fixed with 4% paraformaldehyde and mounted with Vectashield containing DAPI (Vector Laboratories, Inc., UK). Images were taken with an Axioplan2 Imaging fluorescence microscope (Zeiss, Germany) equipped with a DC350FX camera (Zeiss, Germany) and processed using Adobe Photoshop (Adobe Systems, USA).

Double immunofluorescence labelling of rat retinas

Unfixed eyes of 20 day old (P20) Wistar rats were isolated and frozen in melting isopentane. Cryosections were made at a thickness of 7 µm and treated with 0.01% Tween-20 in PBS followed by a blocking step with blocking solution (0.1% ovalbumin, 0.5% fish gelatin in PBS). Antibodies diluted in blocking solution were incubated overnight at 4°C. Secondary antibodies were also diluted in blocking solution and incubated in the dark for 1 hour. Sections were embedded with Prolong Gold Anti-fade (Molecular Probes, USA). Pictures

were made with an Axioskop2 Mot plus fluorescence microscope (Zeiss, Germany) equipped with an AxioCam MRC5 camera (Zeiss, Germany). Images were processed using Axiovision 4.3 (Zeiss, Germany) and Adobe Photoshop (Adobe Systems, USA).

Pre-embedding immunoelectron microscopy

Immunoelectron microscopy was performed on isolated mouse eyes as previously described (21). In short, vibratome sections through mouse retina were stained by primary antibodies against Nlp and visualized by appropriate secondary antibodies (Vectastain ABC-Kit, Vector, UK). After fixation with 0.5% OsO₄ specimens were embedded in araldite and ultrathin sections were analyzed with a FEI Tecnai 12 Biotwin transmission electron microscope (FEI, The Netherlands).

Acknowledgements

The authors would like to thank Jaap Oostrik and Saskia van der Velde-Visser and Elisabeth Sehn for technical assistance, Dr. Pascal Duijf for providing us with the pBD-*p63* vector and Dr. Erich Nigg for providing us with the antibody against Nlp. This work was supported by grants from the British Retinitis Pigmentosa Society (to H.K. and R.R.), the DFG (to U.W.), Forschung contra Blindheit - Initiative Usher Syndrom (to H.K., T.M. and U.W.), ProRetina Deutschland (to U.W. and R.R.), the FAUN-Stiftung, Nürnberg (U.W.), the Heinsius Houbolt Foundation (to H.K.), the Netherlands Organisation for Scientific Research (VIDI 917.86.396, to R.R.), the European Commission IP “EVI-GenoRet” LSHG-CT-2005-512036, the Foundation for Retinal Research, the Algemene Nederlandse Vereniging ter Voorkoming van Blindheid, the Stichting Blindenhulp, the Stichting OOG, and the Rotterdamse Vereniging Blindenbelangen (to F.P.M.C. and R.R.).

Conflict of Interest statement: There are no conflicts of interest.

References

1. Marazita, M.L., Ploughman, L.M., Rawlings, B., Remington, E., Arnos, K.S., and Nance, W.E. (1993) Genetic epidemiological studies of early-onset deafness in the U.S. school-age population. *Am.J.Med.Genet.*, **46**, 486-491.
2. Spandau, U.H., Rohrschneider, K. (2002) Prevalence and geographical distribution of Usher syndrome in Germany. *Graefes Arch.Clin.Exp.Ophthalmol.*, **240**, 495-498.
3. Rosenberg, T., Haim, M., Hauch, A.M., and Parving, A. (1997) The prevalence of Usher syndrome and other retinal dystrophy-hearing impairment associations. *Clin.Genet.*, **51**, 314-321.
4. Smith, R.J., Berlin, C.I., Hejtmancik, J.F., Keats, B.J., Kimberling, W.J., Lewis, R.A., Moller, C.G., Pelias, M.Z., and Tranebjaerg, L. (1994) Clinical diagnosis of the Usher syndromes. Usher Syndrome Consortium. *Am.J.Med.Genet.*, **50**, 32-38.
5. Kremer, H., van Wijk, E., Maerker, T., Wolfrum, U., and Roepman, R. (2006) Usher syndrome: molecular links of pathogenesis, proteins and pathways. *Hum.Mol.Genet.*, **15 Spec No 2**, R262-R270.
6. Weil, D., Blanchard, S., Kaplan, J., Guilford, P., Gibson, F., Walsh, J., Mburu, P., Varela, A., Levilliers, J., Weston, M.D., and . (1995) Defective myosin VIIA gene responsible for Usher syndrome type 1B. *Nature*, **374**, 60-61.
7. Verpy, E., Leibovici, M., Zwaenepoel, I., Liu, X.Z., Gal, A., Salem, N., Mansour, A., Blanchard, S., Kobayashi, I., Keats, B.J., Slim, R., and Petit, C. (2000) A defect in harmonin, a PDZ domain-containing protein expressed in the inner ear sensory hair cells, underlies Usher syndrome type 1C. *Nat.Genet.*, **26**, 51-55.
8. Bork, J.M., Peters, L.M., Riazuddin, S., Bernstein, S.L., Ahmed, Z.M., Ness, S.L., Polomeno, R., Ramesh, A., Schloss, M., Srisailpathy, C.R., Wayne, S., Bellman, S., Desmukh, D., Ahmed, Z., Khan, S.N., Kaloustian, V.M., Li, X.C., Lalwani, A., Riazuddin, S., Bitner-Glindzicz, M., Nance, W.E., Liu, X.Z., Wistow, G., Smith, R.J., Griffith, A.J., Wilcox, E.R., Friedman, T.B., and Morell, R.J. (2001) Usher syndrome 1D and nonsyndromic autosomal recessive deafness DFNB12 are caused by allelic mutations of the novel cadherin-like gene CDH23. *Am.J.Hum.Genet.*, **68**, 26-37.
9. Ahmed, Z.M., Riazuddin, S., Bernstein, S.L., Ahmed, Z., Khan, S., Griffith, A.J., Morell, R.J., Friedman, T.B., Riazuddin, S., and Wilcox, E.R. (2001) Mutations of the protocadherin gene PCDH15 cause Usher syndrome type 1F. *Am.J.Hum.Genet.*, **69**, 25-34.
10. Weil, D., El Amraoui, A., Masmoudi, S., Mustapha, M., Kikkawa, Y., Laine, S., Delmaghani, S., Adato, A., Nadifi, S., Zina, Z.B., Hamel, C., Gal, A., Ayadi, H., Yonekawa, H., and Petit, C. (2003) Usher syndrome type I G (USH1G) is caused by mutations in the gene encoding SANS, a protein that associates with the USH1C protein, harmonin. *Hum.Mol.Genet.*, **12**, 463-471.
11. Bolz, H., von Brederlow, B., Ramirez, A., Bryda, E.C., Kutsche, K., Nothwang, H.G., Seeliger, M., del, C.-S., Vila, M.C., Molina, O.P., Gal, A., and Kubisch, C. (2001)

Mutation of CDH23, encoding a new member of the cadherin gene family, causes Usher syndrome type 1D. *Nat.Genet.*, **27**, 108-112.

12. van Wijk,E., Pennings,R.J., te Brinke,H., Claassen,A., Yntema,H.G., Hoefsloot,L.H., Cremers,F.P.M., Cremers,C.W.R.J., and Kremer,H. (2004) Identification of 51 novel exons of the Usher syndrome type 2A (USH2A) gene that encode multiple conserved functional domains and that are mutated in patients with Usher syndrome type II. *Am.J.Hum.Genet.*, **74**, 738-744.
13. Eudy,J.D., Weston,M.D., Yao,S., Hoover,D.M., Rehm,H.L., Ma-Edmonds,M., Yan,D., Ahmad,I., Cheng,J.J., Ayuso,C., Cremers,C., Davenport,S., Moller,C., Talmadge,C.B., Beisel,K.W., Tamayo,M., Morton,C.C., Swaroop,A., Kimberling,W.J., and Sumegi,J. (1998) Mutation of a gene encoding a protein with extracellular matrix motifs in Usher syndrome type IIa. *Science*, **280**, 1753-1757.
14. Weston,M.D., Luijendijk,M.W., Humphrey,K.D., Moller,C., and Kimberling,W.J. (2004) Mutations in the VLGR1 gene implicate G-protein signaling in the pathogenesis of Usher syndrome type II. *Am.J.Hum.Genet.*, **74**, 357-366.
15. Ebermann,I., Scholl,H.P., Charbel,I.P., Becirovic,E., Lamprecht,J., Jurklics,B., Millan,J.M., Aller,E., Mitter,D., and Bolz,H. (2007) A novel gene for Usher syndrome type 2: mutations in the long isoform of whirlin are associated with retinitis pigmentosa and sensorineural hearing loss. *Hum.Genet.*, **121**, 203-211.
16. Joensuu,T., Hamalainen,R., Yuan,B., Johnson,C., Tegelberg,S., Gasparini,P., Zelante,L., Pirvola,U., Pakarinen,L., Lehesjoki,A.E., de la,C.A., and Sankila,E.M. (2001) Mutations in a novel gene with transmembrane domains underlie Usher syndrome type 3. *Am.J.Hum.Genet.*, **69**, 673-684.
17. Reiners,J., van Wijk,E., Maerker,T., Zimmermann,U., Jurgens,K., te Brinke,H., Overlack,N., Roepman,R., Knipper,M., Kremer,H., and Wolfrum,U. (2005) Scaffold protein harmonin (USH1C) provides molecular links between Usher syndrome type 1 and type 2. *Hum.Mol.Genet.*, **14**, 3933-3943.
18. Adato,A., Michel,V., Kikkawa,Y., Reiners,J., Alagramam,K.N., Weil,D., Yonekawa,H., Wolfrum,U., El Amraoui,A., and Petit,C. (2005) Interactions in the network of Usher syndrome type 1 proteins. *Hum.Mol.Genet.*, **14**, 347-356.
19. van Wijk,E., van der Zwaag,B., Peters,T., Zimmermann,U., te Brinke,H., Kersten,F.F.J., Maerker,T., Aller,E., Hoefsloot,L.H., Cremers,C.W.R.J., Cremers,F.P.M., Wolfrum,U., Knipper,M., Roepman,R., and Kremer,H. (2006) The DFNB31 gene product whirlin connects to the Usher protein network in the cochlea and retina by direct association with USH2A and VLGR1. *Hum.Mol.Genet.*, **15**, 751-765.
20. Boeda,B., El Amraoui,A., Bahloul,A., Goodyear,R., Daviet,L., Blanchard,S., Perfettini,I., Fath,K.R., Shorte,S., Reiners,J., Houdusse,A., Legrain,P., Wolfrum,U., Richardson,G., and Petit,C. (2002) Myosin VIIa, harmonin and cadherin 23, three Usher I gene products that cooperate to shape the sensory hair cell bundle. *EMBO J.*, **21**, 6689-6699.

21. Maerker,T., van Wijk,E., Overlack,N., Kersten,F.F.J., McGee,J., Goldmann,T., Sehn,E., Roepman,R., Walsh,E.J., Kremer,H., and Wolfrum,U. (2008) A novel Usher protein network at the periciliary reloading point between molecular transport machineries in vertebrate photoreceptor cells. *Hum.Mol.Genet.*, **17**, 71-86.
22. Adato,A., Lefevre,G., Delprat,B., Michel,V., Michalski,N., Chardenoux,S., Weil,D., El Amraoui,A., and Petit,C. (2005) Usherin, the defective protein in Usher syndrome type IIA, is likely to be a component of interstereocilia ankle links in the inner ear sensory cells. *Hum.Mol.Genet.*, **14**, 3921-3932.
23. Liu,X., Bulgakov,O.V., Darrow,K.N., Pawlyk,B., Adamian,M., Liberman,M.C., and Li,T. (2007) Usherin is required for maintenance of retinal photoreceptors and normal development of cochlear hair cells. *Proc.Natl.Acad.Sci.U.S.A.*, **104**, 4413-4418.
24. Hunter,D.G., Fishman,G.A., Mehta,R.S., and Kretzer,F.L. (1986) Abnormal sperm and photoreceptor axonemes in Usher's syndrome. *Arch.Ophthalmol.*, **104**, 385-389.
25. Adams,N.A., Awadein,A., and Toma,H.S. (2007) The retinal ciliopathies. *Ophthalmic Genet.*, **28**, 113-125.
26. Jacobson,S.G., Cideciyan,A.V., Aleman,T.S., Sumaroka,A., Roman,A.J., Gardner,L.M., Prosser,H.M., Mishra,M., Bech-Hansen,N.T., Herrera,W., Schwartz,S.B., Liu,X.Z., Kimberling,W.J., Steel,K.P., and Williams,D.S. (2008) Usher syndromes due to MYO7A, PCDH15, USH2A or GPR98 mutations share retinal disease mechanism. *Hum.Mol.Genet.*
27. Leber,T. (1869) Uber retinitis pigmentosa und angebore amaurose. *Graefes Arch.Clin.Exp.Ophthalmol.*, **15**, 1-25.
28. Franceschetti,A., Dieterle,P. (1954) Diagnostic and prognostic importance of the electroretinogram in tapetoretinal degeneration with reduction of the visual field and hemeralopia. *Confin.Neurol.*, **14**, 184-186.
29. den Hollander,A.I., Koenekoop,R.K., Mohamed,M.D., Arts,H.H., Boldt,K., Towns,K.V., Sedmak,T., Beer,M., Nagel-Wolfrum,K., McKibbin,M., Dharmaraj,S., Lopez,I., Ivings,L., Williams,G.A., Springell,K., Woods,C.G., Jafri,H., Rashid,Y., Strom,T.M., van der Zwaag,B., Gosens,I., Kersten,F.F.J., van Wijk,E., Veltman,J.A., Zonneveld,M.N., van Beersum,S.E.C., Maumenee,I.H., Wolfrum,U., Cheetham,M.E., Ueffing,M., Cremers,F.P.M., Inglehearn,C.F., and Roepman,R. (2007) Mutations in LCA5, encoding the ciliary protein lebercilin, cause Leber congenital amaurosis. *Nat.Genet.*, **39**, 889-895.
30. den Hollander,A.I., Koenekoop,R.K., Yzer,S., Lopez,I., Arends,M.L., Voeselek,K.E., Zonneveld,M.N., Strom,T.M., Meitinger,T., Brunner,H.G., Hoyng,C.B., van den Born,L.I., Rohrschneider,K., and Cremers,F.P.M. (2006) Mutations in the CEP290 (NPHP6) gene are a frequent cause of Leber congenital amaurosis. *Am.J.Hum.Genet.*, **79**, 556-561.
31. Arts,H.H., Cremers,F.P.M., Knoers,N.V.A.M., and Roepman,R. (2008) Focus on Molecules: RPGRIP1. *Exp.Eye Res.*

32. Casenghi,M., Meraldi,P., Weinhart,U., Duncan,P.I., Korner,R., and Nigg,E.A. (2003) Polo-like kinase 1 regulates Nlp, a centrosome protein involved in microtubule nucleation. *Dev.Cell*, **5**, 113-125.
33. Trojan,P., Krauss,N., Choe,H.W., Giessl,A., Pulvermuller,A., and Wolfrum,U. (2008) Centrioles in retinal photoreceptor cells: Regulators in the connecting cilium. *Prog.Retin.Eye Res.*, **27**, 237-259.
34. Grabarek,Z. (2005) Structure of a trapped intermediate of calmodulin: calcium regulation of EF-hand proteins from a new perspective. *J.Mol.Biol.*, **346**, 1351-1366.
35. Cohen,E., Binet,S., and Meininger,V. (1988) Ciliogenesis and centriole formation in the mouse embryonic nervous system. An ultrastructural analysis. *Biol.Cell*, **62**, 165-169.
36. Rapley,J., Baxter,J.E., Blot,J., Wattam,S.L., Casenghi,M., Meraldi,P., Nigg,E.A., and Fry,A.M. (2005) Coordinate regulation of the mother centriole component nlp by nek2 and plk1 protein kinases. *Mol.Cell Biol.*, **25**, 1309-1324.
37. Casenghi,M., Barr,F.A., and Nigg,E.A. (2005) Phosphorylation of Nlp by Plk1 negatively regulates its dynein-dynactin-dependent targeting to the centrosome. *J.Cell Sci.*, **118**, 5101-5108.
38. Roepman,R., Wolfrum,U. (2007) Protein networks and complexes in photoreceptor cilia. *Subcell.Biochem.*, **43**, 209-235.
39. Besharse,J.C., Horst,C.J. (1990) In Bloodgood,R.A. (ed), Ciliary and flagellar membranes. Plenum, New York, pp. 389-417.
40. Reiners,J., Nagel-Wolfrum,K., Jurgens,K., Maerker,T., and Wolfrum,U. (2006) Molecular basis of human Usher syndrome: deciphering the meshes of the Usher protein network provides insights into the pathomechanisms of the Usher disease. *Exp.Eye Res.*, **83**, 97-119.
41. Barrong,S.D., Chaitin,M.H., Fliesler,S.J., Possin,D.E., Jacobson,S.G., and Milam,A.H. (1992) Ultrastructure of connecting cilia in different forms of retinitis pigmentosa. *Arch.Ophthalmol.*, **110**, 706-710.
42. Dryja,T.P., Adams,S.M., Grimsby,J.L., McGee,T.L., Hong,D.H., Li,T., Andreasson,S., and Berson,E.L. (2001) Null RPGRIP1 alleles in patients with Leber congenital amaurosis. *Am.J.Hum.Genet.*, **68**, 1295-1298.
43. Liu,Q., Zhou,J., Daiger,S.P., Farber,D.B., Heckenlively,J.R., Smith,J.E., Sullivan,L.S., Zuo,J., Milam,A.H., and Pierce,E.A. (2002) Identification and subcellular localization of the RP1 protein in human and mouse photoreceptors. *Invest Ophthalmol.Vis.Sci.*, **43**, 22-32.
44. Liu,Q., Zuo,J., and Pierce,E.A. (2004) The retinitis pigmentosa 1 protein is a photoreceptor microtubule-associated protein. *J.Neurosci.*, **24**, 6427-6436.
45. Iannaccone,A., Breuer,D.K., Wang,X.F., Kuo,S.F., Normando,E.M., Filippova,E., Baldi,A., Hiriyantha,S., MacDonald,C.B., Baldi,F., Cosgrove,D., Morton,C.C.,

- Swaroop,A., and Jablonski,M.M. (2003) Clinical and immunohistochemical evidence for an X linked retinitis pigmentosa syndrome with recurrent infections and hearing loss in association with an RPGR mutation. *J.Med.Genet.*, **40**, e118.
46. Hong,D.H., Yue,G., Adamian,M., and Li,T. (2001) Retinitis pigmentosa GTPase regulator (RPGRr)-interacting protein is stably associated with the photoreceptor ciliary axoneme and anchors RPGR to the connecting cilium. *J.Biol.Chem.*, **276**, 12091-12099.
 47. Rosenbaum,J.L., Witman,G.B. (2002) Intraflagellar transport. *Nat.Rev.Mol.Cell Biol.*, **3**, 813-825.
 48. Wolfrum,U., Schmitt,A. (2000) Rhodopsin transport in the membrane of the connecting cilium of mammalian photoreceptor cells. *Cell Motil.Cytoskeleton*, **46**, 95-107.
 49. Pazour,G.J., Dickert,B.L., and Witman,G.B. (1999) The DHC1b (DHC2) isoform of cytoplasmic dynein is required for flagellar assembly. *J.Cell Biol.*, **144**, 473-481.
 50. Pedersen,L.B., Miller,M.S., Geimer,S., Leitch,J.M., Rosenbaum,J.L., and Cole,D.G. (2005) Chlamydomonas IFT172 is encoded by FLA11, interacts with CrEB1, and regulates IFT at the flagellar tip. *Curr.Biol.*, **15**, 262-266.
 51. Kozminski,K.G., Beech,P.L., and Rosenbaum,J.L. (1995) The Chlamydomonas kinesin-like protein FLA10 is involved in motility associated with the flagellar membrane. *J.Cell Biol.*, **131**, 1517-1527.
 52. Evans,J.E., Snow,J.J., Gunnarson,A.L., Ou,G., Stahlberg,H., McDonald,K.L., and Scholey,J.M. (2006) Functional modulation of IFT kinesins extends the sensory repertoire of ciliated neurons in *Caenorhabditis elegans*. *J.Cell Biol.*, **172**, 663-669.
 53. Pazour,G.J., Baker,S.A., Deane,J.A., Cole,D.G., Dickert,B.L., Rosenbaum,J.L., Witman,G.B., and Besharse,J.C. (2002) The intraflagellar transport protein, IFT88, is essential for vertebrate photoreceptor assembly and maintenance. *J.Cell Biol.*, **157**, 103-113.
 54. Baker,S.A., Freeman,K., Luby-Phelps,K., Pazour,G.J., and Besharse,J.C. (2003) IFT20 links kinesin II with a mammalian intraflagellar transport complex that is conserved in motile flagella and sensory cilia. *J.Biol.Chem.*, **278**, 34211-34218.
 55. Insinna,C., Pathak,N., Perkins,B., Drummond,I., and Besharse,J.C. (2008) The homodimeric kinesin, Kif17, is essential for vertebrate photoreceptor sensory outer segment development. *Dev.Biol.*, **316**, 160-170.
 56. Marszalek,J.R., Liu,X., Roberts,E.A., Chui,D., Marth,J.D., Williams,D.S., and Goldstein,L.S. (2000) Genetic evidence for selective transport of opsin and arrestin by kinesin-II in mammalian photoreceptors. *Cell*, **102**, 175-187.
 57. Pazour,G.J., Dickert,B.L., Vucica,Y., Seeley,E.S., Rosenbaum,J.L., Witman,G.B., and Cole,D.G. (2000) Chlamydomonas IFT88 and its mouse homologue, polycystic kidney disease gene *tg737*, are required for assembly of cilia and flagella. *J.Cell Biol.*, **151**, 709-718.

58. Abd-El-Barr,M.M., Sykoudis,K., Andrabi,S., Eichers,E.R., Pennesi,M.E., Tan,P.L., Wilson,J.H., Katsanis,N., Lupski,J.R., and Wu,S.M. (2007) Impaired photoreceptor protein transport and synaptic transmission in a mouse model of Bardet-Biedl syndrome. *Vision Res.*, **47**, 3394-3407.
59. Nachury,M.V., Loktev,A.V., Zhang,Q., Westlake,C.J., Peranen,J., Merdes,A., Slusarski,D.C., Scheller,R.H., Bazan,J.F., Sheffield,V.C., and Jackson,P.K. (2007) A core complex of BBS proteins cooperates with the GTPase Rab8 to promote ciliary membrane biogenesis. *Cell*, **129**, 1201-1213.
60. Overlack,N., Maerker,T., Latz,M., Nagel-Wolfrum,K., and Wolfrum,U. (2008) SANS (USH1G) expression in developing and mature mammalian retina. *Vision Res.*, **48**, 400-412.
61. Liu,X., Udovichenko,I.P., Brown,S.D., Steel,K.P., and Williams,D.S. (1999) Myosin VIIa participates in opsin transport through the photoreceptor cilium. *J.Neurosci.*, **19**, 6267-6274.
62. Follit,J.A., Tuft,R.A., Fogarty,K.E., and Pazour,G.J. (2006) The intraflagellar transport protein IFT20 is associated with the Golgi complex and is required for cilia assembly. *Mol.Biol.Cell*, **17**, 3781-3792.
63. Papermaster,D.S. (2002) The birth and death of photoreceptors: the Friedenwald Lecture. *Invest Ophthalmol.Vis.Sci.*, **43**, 1300-1309.
64. Tai,A.W., Chuang,J.Z., Bode,C., Wolfrum,U., and Sung,C.H. (1999) Rhodopsin's carboxy-terminal cytoplasmic tail acts as a membrane receptor for cytoplasmic dynein by binding to the dynein light chain Tctex-1. *Cell*, **97**, 877-887.
65. Reiter,J.F., Mostov,K. (2006) Vesicle transport, cilium formation, and membrane specialization: the origins of a sensory organelle. *Proc.Natl.Acad.Sci.U.S.A*, **103**, 18383-18384.
66. Zhang,H., Shi,X., Paddon,H., Hampong,M., Dai,W., and Pelech,S. (2004) B23/nucleophosmin serine 4 phosphorylation mediates mitotic functions of polo-like kinase 1. *J.Biol.Chem.*, **279**, 35726-35734.
67. Shinmura,K., Tarapore,P., Tokuyama,Y., George,K.R., and Fukasawa,K. (2005) Characterization of centrosomal association of nucleophosmin/B23 linked to Crm1 activity. *FEBS Lett.*, **579**, 6621-6634.
68. Shu,X., Fry,A.M., Tulloch,B., Manson,F.D., Crabb,J.W., Khanna,H., Faragher,A.J., Lennon,A., He,S., Trojan,P., Giessl,A., Wolfrum,U., Vervoort,R., Swaroop,A., and Wright,A.F. (2005) RPGR ORF15 isoform co-localizes with RPGRIP1 at centrioles and basal bodies and interacts with nucleophosmin. *Hum.Mol.Genet.*, **14**, 1183-1197.
69. Khanna,H., Hurd,T.W., Lillo,C., Shu,X., Parapuram,S.K., He,S., Akimoto,M., Wright,A.F., Margolis,B., Williams,D.S., and Swaroop,A. (2005) RPGR-ORF15, which is mutated in retinitis pigmentosa, associates with SMC1, SMC3, and microtubule transport proteins. *J.Biol.Chem.*, **280**, 33580-33587.

70. Roepman,R., Schick,D., and Ferreira,P.A. (2000) Isolation of retinal proteins that interact with retinitis pigmentosa GTPase regulator by interaction trap screen in yeast. *Methods Enzymol.*, **316**, 688-704.
71. James,P., Halladay,J., and Craig,E.A. (1996) Genomic libraries and a host strain designed for highly efficient two-hybrid selection in yeast. *Genetics*, **144**, 1425-1436.
72. Luijendijk,M.W., van de Pol,T.J., van Duijnhoven,G., den Hollander,A.I., ten Caat,J., van,L., V, Brunner,H.G., Kremer,H., and Cremers,F.P.M. (2003) Cloning, characterization, and mRNA expression analysis of novel human fetal cochlear cDNAs. *Genomics*, **82**, 480-490.
73. Maruyama,K., Mikawa,T., and Ebashi,S. (1984) Detection of calcium binding proteins by ⁴⁵Ca autoradiography on nitrocellulose membrane after sodium dodecyl sulfate gel electrophoresis. *J.Biochem.(Tokyo)*, **95**, 511-519.

Figure legends

Figure 1:

Schematic representation of the protein structure of Nlp^{isoA} and Nlp^{isoB}. (A) The predicted EF hands (EF) 1, 2 and 3 are formed by amino acids 11-39, 200-228 and 237-265, respectively. Coiled-coil domains (CC) 1, 2, 3 and 4 are formed by amino acids 384-425, 470-579, 621-699 and 1046-1375, respectively, and the predicted intermediate filament domain (IF) is formed by amino acids 656-925. (B) Semi-quantitative RT-PCR for transcripts encoding Nlp^{isoA} and Nlp^{isoB} in human fetal and adult tissues. Shown are the samples that were taken after 35 cycles. The results are representative for the samples taken after 25 and 30 cycles. As a control, RT-PCR analysis of the household gene *GAPDH* was performed. The transcripts for Nlp^{isoA} and Nlp^{isoB} show a similar distribution with the strongest expression in fetal cochlea and adult brain, testis and kidney.

Figure 2:

Protein-protein interaction studies. (A) The schematic protein structure of Nlp^{isoB} and protein fragments encoded by deletion constructs with the corresponding amino acids are depicted. Yeast two-hybrid analysis showed a specific interaction between the fragment of the intracellular region of USH2A^{isoB} encompassing aa 5124-5196 and the predicted intermediate filament domain (aa 656-925) of Nlp^{isoB}. (B) Schematic representation of the protein structure of lebercilin and protein fragments encoded by deletion constructs with the corresponding amino acids. Yeast two-hybrid analysis revealed a specific interaction between the lebercilin domain containing the two N-terminal coiled-coil domains (aa 96-305) and the predicted intermediate filament domain of Nlp^{isoB} (aa 656-925). A liquid beta-galactosidase assay revealed a specific interaction between Nlp^{isoB} and the USH2A_{tail} (C) and Nlp^{isoB} and lebercilin (D). No interaction was observed between USH2A and Nlp^{isoA} (C), and lebercilin and Nlp^{isoA} (D). aa: amino acids; NA: not assayed.

Figure 3:

Co-immunoprecipitation of Nlp^{isoB} with the intracellular region of USH2A^{isoB} (USH2A_{tail}), but not with STRAD. (A) The immunoblot (IB) in the left upper panel shows that HA-Nlp^{isoB} (lane 1) co-immunoprecipitated with flag-USH2A_{tail}, but not with the unrelated protein flag-STRAD (lane 2). Protein input is shown in the left lower panel; the anti-flag immunoprecipitates are shown in the right panel. (B) GST-pull down assays showing that flag-tagged lebercilin was efficiently pulled down by GST-fused Nlp^{isoB}, but not by GST alone. The left lane shows 2% input of the protein lysate. (C) Co-immunoprecipitation of lebercilin with Nlp^{isoB}, but not with LRRK2. The immunoblot (IB) in the right panel shows

that flag-Nlp^{isoB} (right lane) co-immunoprecipitated with HA-lebercilin, whereas the unrelated protein flag-LRRK2 (left lane) did not. Protein input is shown in the left panel; the anti-HA immunoprecipitates are shown in the middle panel. **(D)** Co-immunoprecipitation of endogenous Nlp with lebercilin from bovine retinal extracts, but not with rabbit IgGs. The top panel shows that Nlp was co-immunoprecipitated with lebercilin, indicated by an arrow, whereas it was not with rabbit IgGs. The bottom panel shows that lebercilin was immunoprecipitated with lebercilin-specific antibodies, as indicated by an arrow, but not with rabbit IgGs.

Figure 4:

Analysis of Ca²⁺-binding properties of Nlp. **(A)** Multiple protein alignment of the predicted EF hand domains in Nlp and the consensus sequence for EF hand domains (SMART database). The invariable D or E at position 12 is boxed and indicated by an arrow and is only present in EF hand 3. **(B)** A calcium-binding assay showing the specific calcium-binding capacities of Nlp EF hand 3. The 28K subunit of calmodulin was used as a positive control. **(C)** GST-pull down analysis showing that HA-tagged Nlp^{isoB} was efficiently pulled down by GST-fused USH2A_{tail} in the presence and absence of calcium, but not by GST-NBC3_{tail} and GST alone. Lanes 1 and 5 show 5% of the input protein lysate.

Figure 5:

Co-localization of Nlp and USH2A in the retina. **(A-A'')** Co-immunostaining of USH2A and Nlp in radial cryosections of adult (P20) rat retina by using anti-Nlp antibodies (green signal; **A**) and anti-USH2A antibodies (red signal; **A'**) showing co-localization (yellow signal; **A''**) in the inner segment (IS) and in the region of the connecting cilium (CC). **(B)** High magnification fluorescence microscopy analysis of double immunofluorescence with anti-Nlp (green) and anti-*pan*-centrin antibodies (red; marker for the ciliary apparatus: connecting cilium, centriole and basal body) in cryosections through the ciliary part of rat photoreceptor cells. Merged images indicate partial co-localization of Nlp with centrin in the centriole and basal body (yellow signal). Pre-embedding immunolabelings of the ciliary region of mouse photoreceptors by antibodies against Nlp **(C)** and USH2A^{isoB} **(D)** show a clear staining of the (apical part of) inner segment (IS), the centriole (indicated by an asterisk) and the basal body (BB).

Figure 6:

Centrosomal localization of Nlp^{isoB}, USH2A_{tail} and lebercilin in ARPE-19 cells. When expressed alone, mRFP-Nlp^{isoB} (red signal) was localized to the mother centriole of the centrosome **(A)**, eCFP-USH2A_{tail} (green signal) was localized to the nucleus and the

centrosome (indicated by an arrow and in the inlay) (**B**), whereas eYFP-lebercilin (green signal) was localized at the centrosome and microtubule network of the cell (**C**). After co-expression of Nlp^{isoB} and USH2A both proteins were localized at the mother and daughter centriole of the centrosome, confirming the interaction between both proteins (**D-D''**). Co-expression of Nlp^{isoB} and lebercilin showed co-localization of both proteins at the centrosome and non-centrosomal MTOC's (yellow signal; **E''**). Lebercilin in addition partly localized at the microtubule network (**E-E''**). Nuclei were stained with DAPI (blue signal).

Figure 7:

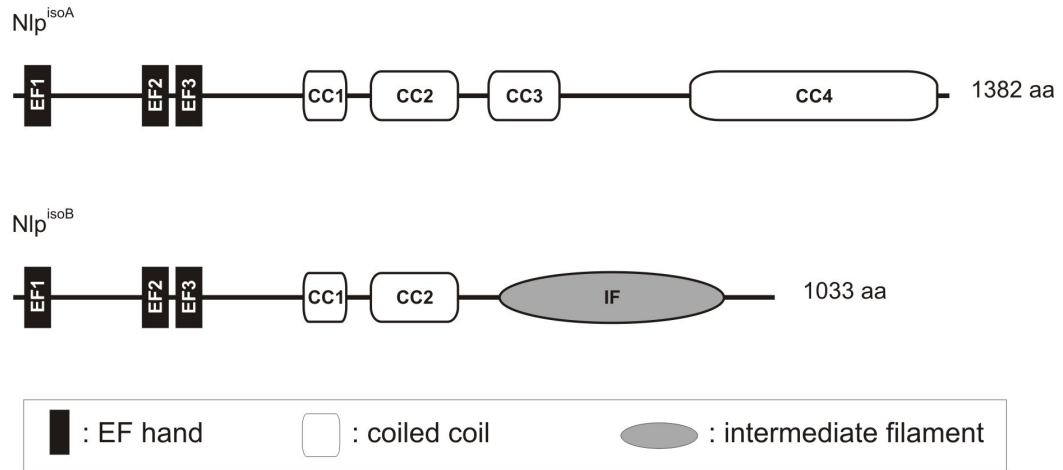
Localization of endogenously expressed Nlp and lebercilin in ARPE-19 cells by immunocytochemistry using the anti-Nlp and anti-lebercilin antibodies (green signals) and anti-acetylated tubulin antibodies as an axoneme and microtubule marker (red signal). Nlp (**A**) and lebercilin (**B**) were present at the basal body of primary cilia and both proteins were found at the midbody region of ARPE-19 cells during telophase (**C** and **D**). Nuclei were stained with DAPI (blue signal).

Figure 8:

Mutations in lebercilin affect the interaction with Nlp^{isoB}. A quantitative liquid beta-galactosidase assay shows an enhanced interaction of Nlp^{isoB} and lebercilin^{Q279X} as compared to wild-type lebercilin, and a reduced interaction of Nlp^{isoB} and lebercilin^{P493TfsX1} (**A**). When expressed alone in ARPE-19 cells, mRFP-lebercilin wild-type (red signal) was localized to the basal body, the primary cilium and microtubule network of the cell (**B**), mRFP-lebercilin^{Q279X} was localized to the basal body and primary cilium (**C**) and mRFP-lebercilin^{P493TfsX1} was localized to the microtubule network of the cell (**D**). Co-expression of Nlp^{isoB} and lebercilin showed co-localization of both proteins at the basal body (yellow signal; **E''**, inset). In addition, lebercilin localized to the primary cilium and the microtubule network in the cell periphery (red signal; **E'-E''**, inset). Upon co-expression of Nlp^{isoB} and lebercilin^{Q279X}, both proteins co-localize at the basal body (yellow signal; **F''**, inset). The mutant lebercilin was not found in the primary cilium (**F'-F''**, inset). After co-expression of Nlp^{isoB} and lebercilin^{P493TfsX1} no co-localization of these proteins was observed (**G-G''**, inset). Nuclei were stained with DAPI (blue signal).

Figure 1

A



B

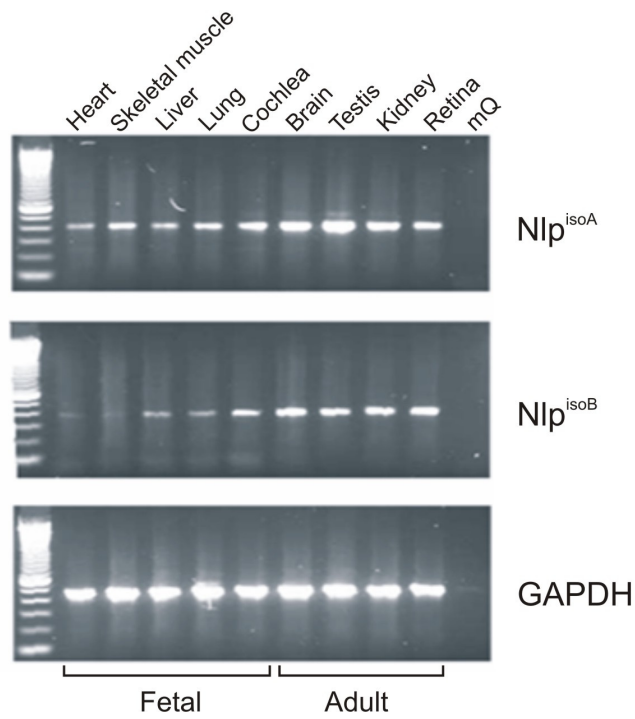
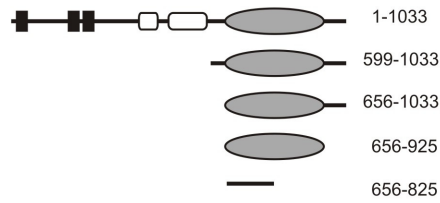


Figure 2

A

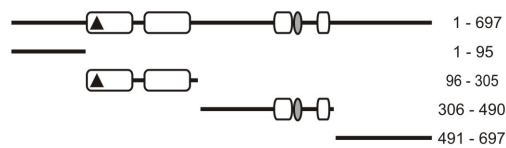
Deletion constructs:



USH2A isoB / Nlp isoB	5064 - 5202	5064 - 5196	5064 - 5168	5124 - 5202	5124 - 5196	5169 - 5202
1-1033	++	++	-	++	++	-
599-1033	+++	+++	-	+++	+++	-
656-1033	+++	NA	NA	NA	NA	NA
656-925	++	NA	NA	NA	NA	NA
656-825	-	NA	NA	NA	NA	NA

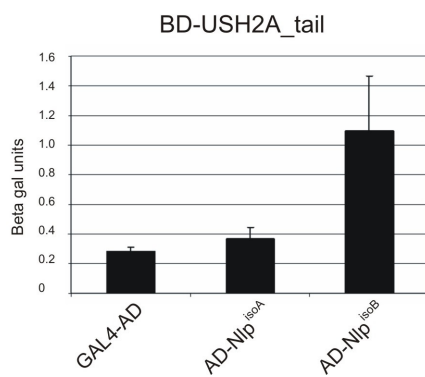
B

Deletion constructs:



Lebercilin / Nlp isoB	1-697	1-95	96-305	306-490	491-697
1-1033	+++	-	+++	-	-
656-1033	+++	NA	+++	NA	NA
656-925	++	NA	++	NA	NA
656-825	-	NA	-	NA	NA

C



D

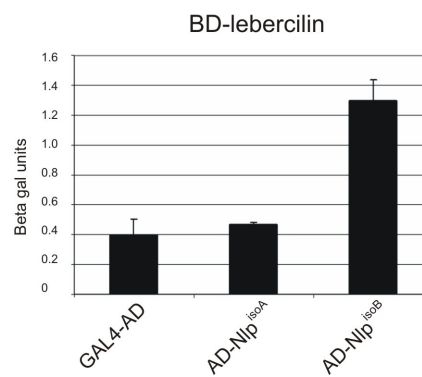
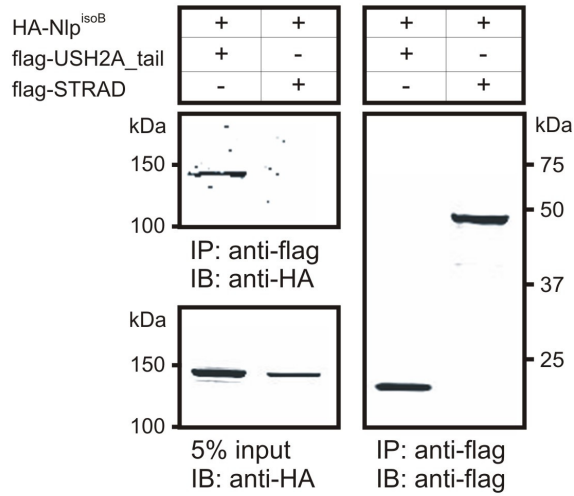
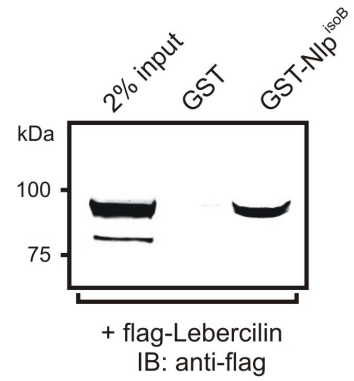


Figure 3

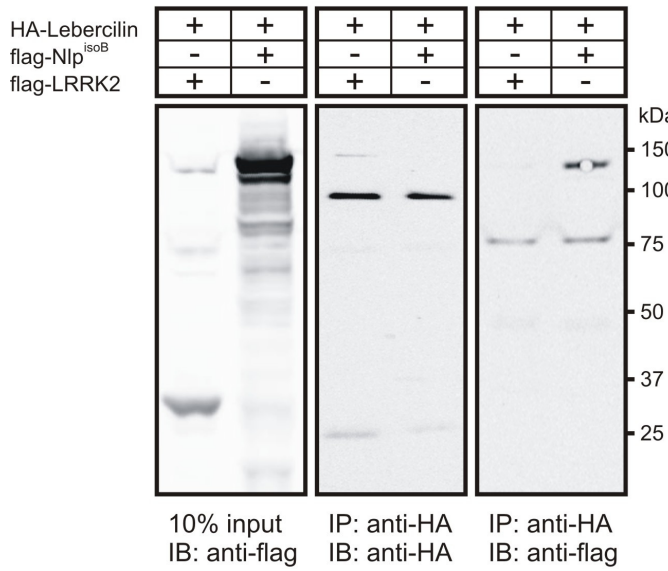
A



B



C



D

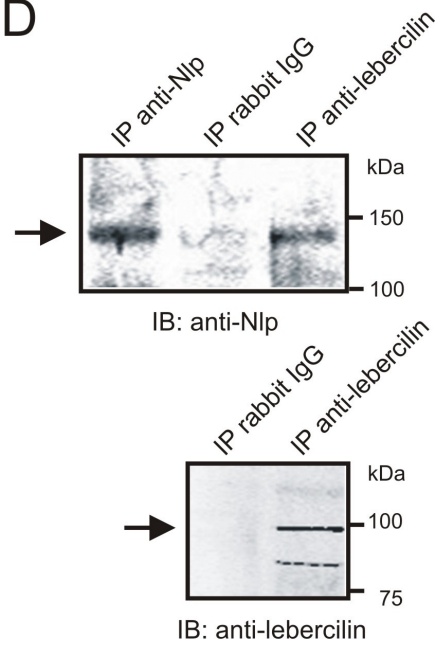


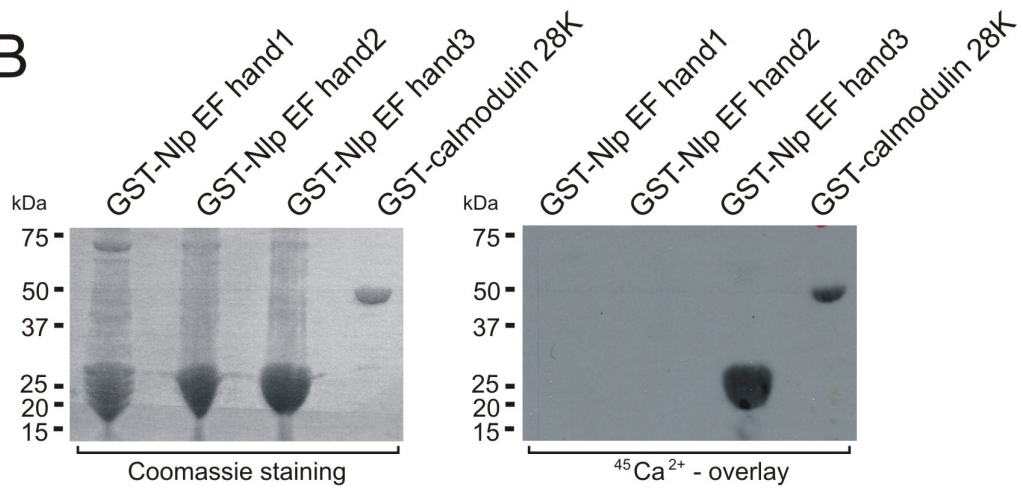
Figure 4

A

Consensus EF hand	EFRASFNHFDRDHS	GLGPEEFKACLISL
Nlp EF hand 1	QLREYVSSCDTIT	GTGFLDRQELTQLCLKL
Nlp EF hand 2	QIRGVWEELGVG	SSGHLSEQELAVVCQSV
Nlp EF hand 3	ELEDLFNKLDQD	DGDGKVSLEEFQLGLFSH

↑

B



C

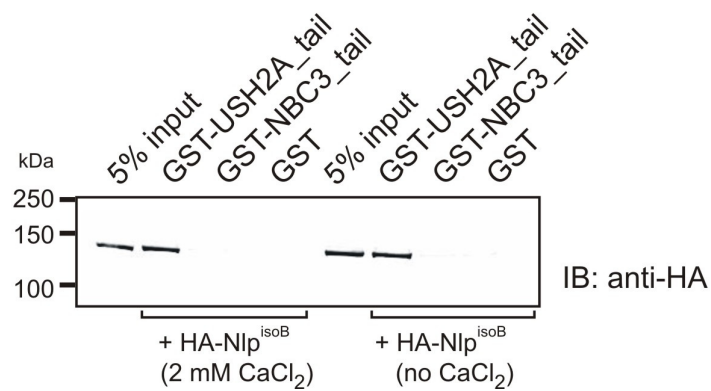


Figure 5

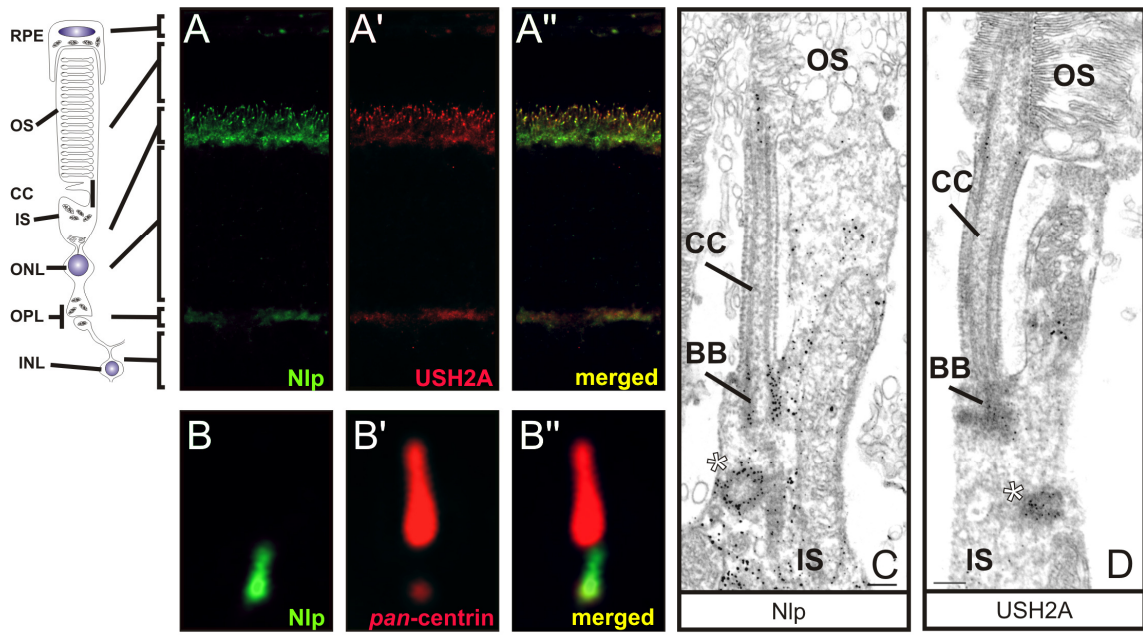


Figure 6

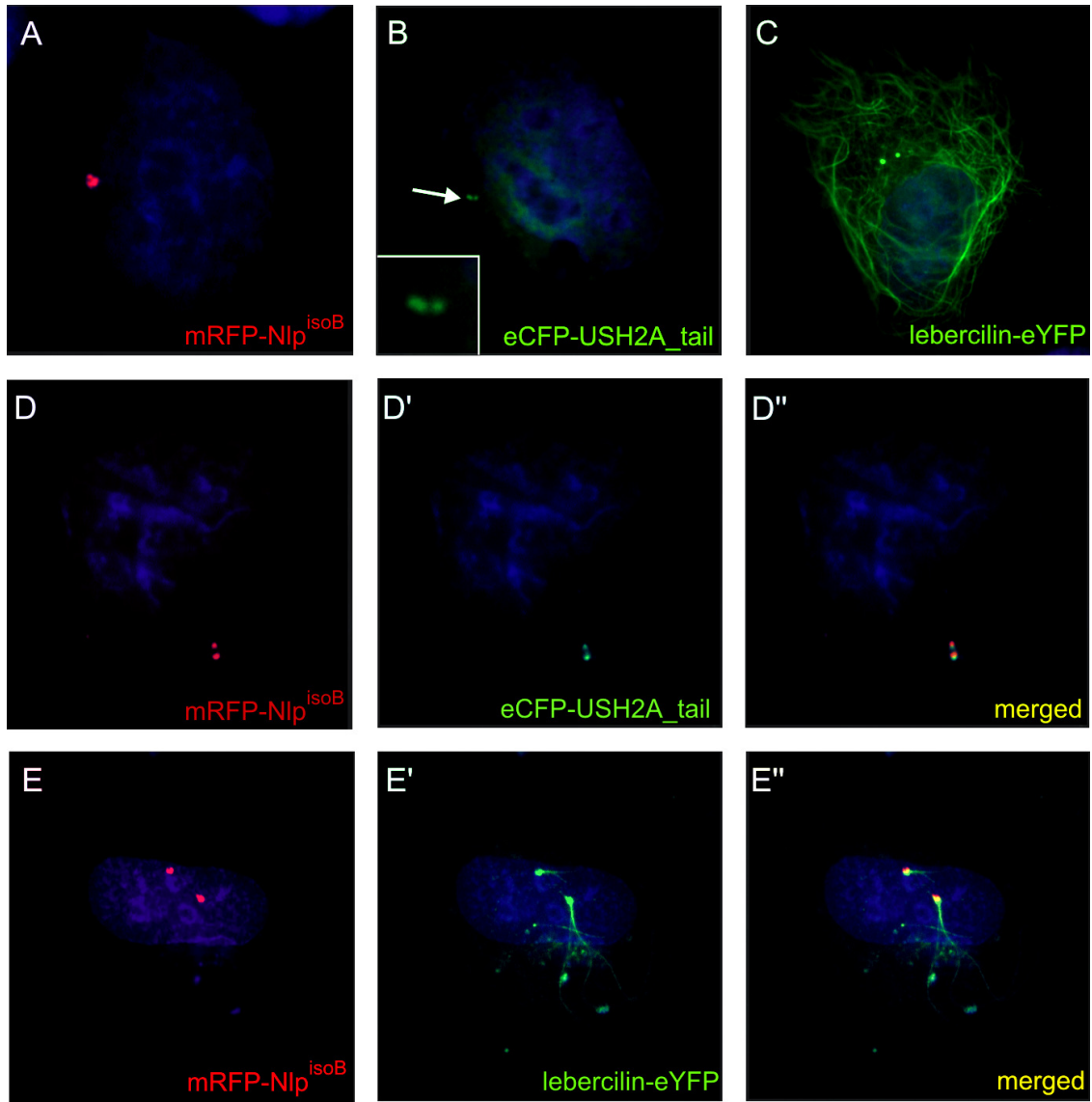


Figure 7

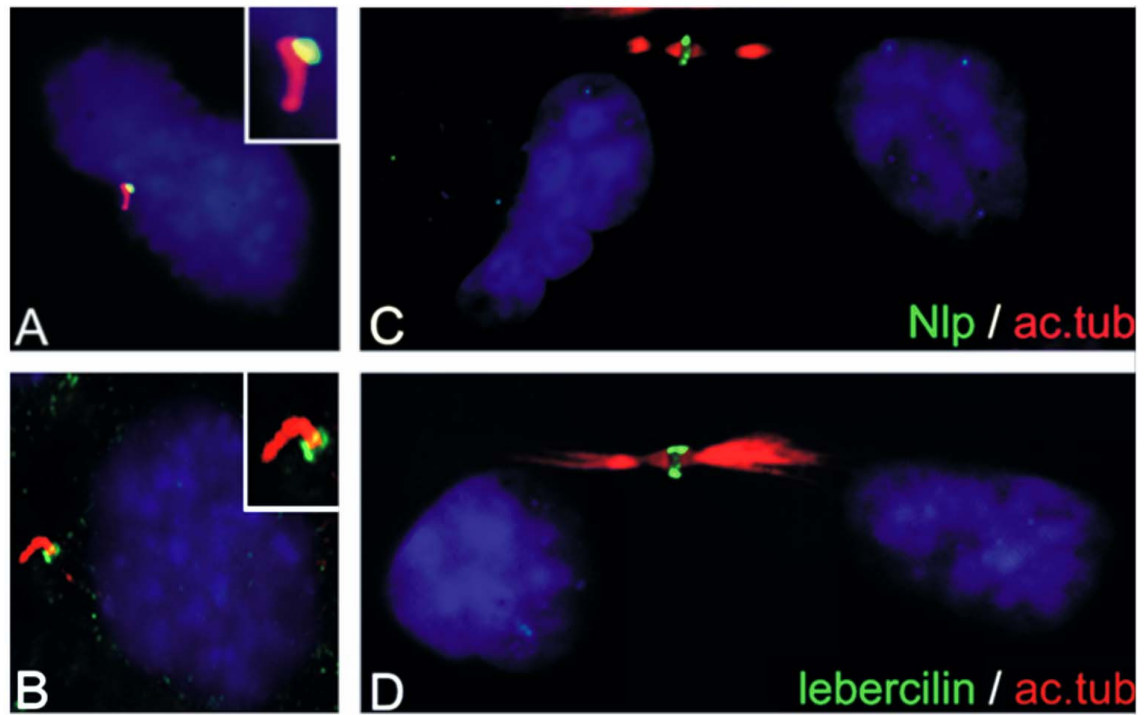


Figure 8

